Brain Stimulation 11 (2018) 849–855

Contents lists available at ScienceDirect

Brain Stimulation

journal homepage: http://www.journals.elsevier.com/brain-stimulation

Multi-locus transcranial magnetic stimulation—theory and implementation

Lari M. Koponen [a, b, 1], Jaakko O. Nieminen [a, b, *, 1], Risto J. Ilmoniemi [a, b]

[a] Department of Neuroscience and Biomedical Engineering, Aalto University School of Science, Espoo, Finland
[b] BioMag Laboratory, HUS Medical Imaging Center, University of Helsinki and Helsinki University Hospital, Helsinki, Finland

ARTICLE INFO

Article history:
Received 3 November 2017
Received in revised form
9 February 2018
Accepted 20 March 2018
Available online 23 March 2018

Keywords:
Transcranial magnetic stimulation
Multi-channel TMS
Multi-locus TMS
Instrumentation
Coil design
Electric field

ABSTRACT

Background: Transcranial magnetic stimulation (TMS) is a non-invasive brain stimulation method: a magnetic field pulse from a TMS coil can excite neurons in a desired location of the cortex. Conventional TMS coils cause focal stimulation underneath the coil centre; to change the location of the stimulated spot, the coil must be moved over the new target. This physical movement is inherently slow, which limits, for example, feedback-controlled stimulation.
Objective: To overcome the limitations of physical TMS-coil movement by introducing electronic targeting.
Methods: We propose electronic stimulation targeting using a set of large overlapping coils and introduce a matrix-factorisation-based method to design such sets of coils. We built one such device and demonstrated the electronic stimulation targeting *in vivo*.
Results: The demonstrated two-coil transducer allows translating the stimulated spot along a 30-mm-long line segment in the cortex; with five coils, a target can be selected from within a region of the cortex and stimulated in any direction. Thus, far fewer coils are required by our approach than by previously suggested ones, none of which have resulted in practical devices.
Conclusion: Already with two coils, we can adjust the location of the induced electric field maximum along one dimension, which is sufficient to study, for example, the primary motor cortex.

Introduction

Transcranial magnetic stimulation (TMS) is a method for non-invasive brain stimulation [1]. It has become an attractive tool in neuroscience [2–4] and in some clinical applications [5,6], with thousands of devices worldwide. In TMS, a strong current pulse through the windings of a coil produces a magnetic field, which, in turn, induces an electric field (E-field) in nearby tissues. With a suitable figure-of-eight coil [7], the cortex can be stimulated locally; a typical modern TMS device has one such coil, held at the desired position above the stimulation target. Neuronavigation technology [8–10], with targeting based on individual anatomical images and with visual feedback to the operator, makes it relatively straightforward to maintain the stimulated spot (i.e., the location of the E-field maximum in the cortex) within a couple of millimetres of its desired location (the stimulation target). Even neuronavigated conventional TMS devices have, however, a major limitation: to change the stimulated spot, the coil must be moved. Moving the heavy (around 1–2 kg) coil, even robotically [11], is relatively slow, as the coil must be close to the scalp during the stimulation and safety has to be guaranteed. Thus, when connectivity between cortical areas has been studied with TMS pulses targeted to them in a sequence, two [12] or sometimes even three [13] distinct coils have been used—one for each stimulation target.

Although multiple spots can be stimulated in quick succession with multiple separate coils, this approach has severe limitations. First, it is cumbersome to manipulate and control several coils at the same time. Second, the large size of the coils makes it difficult to stimulate nearby cortical locations [14,15]. Third, changing any of the stimulated spots still requires a rearrangement of the coil assembly. To overcome these limitations, the concept of an array of small coils has been suggested [8,16]. With such an array, the stimulated spot could, in principle, be changed electronically without moving the coils. The previously proposed approach,

* Corresponding author. Department of Neuroscience and Biomedical Engineering, Aalto University School of Science, P.O. Box 12200, FI-00076 AALTO, Finland.
E-mail address: jaakko.nieminen@aalto.fi (J.O. Nieminen).
[1] These authors contributed equally to this work.

https://doi.org/10.1016/j.brs.2018.03.014

however, would require a large number of coils (a rectangular 4-by-4 lattice of 16 coils, each smaller than 30 mm in diameter, could cover a region slightly smaller than the four central coils) and much more power to drive all the coils than is required for a single conventional TMS coil. Indeed, each such coil would require its own power electronics similar to that of a conventional TMS device. As a TMS device is largely characterised by its power electronics, this essentially means that at least 16 TMS devices would be required to drive such an array. This would make the device both costly and bulky; to our knowledge, no such device has ever been built. The largest multi-channel TMS device described in the literature has five coils and is intended to give multiple simultaneous pulses with different waveforms [17].

In this work, we propose and demonstrate a practical approach to control the stimulated spot within the cortex and provide an algorithm to design multi-locus TMS (mTMS) transducers with overlapping coils. As will be shown in this study, with five such coils, one can select a target location from within a region of the cortex and stimulate it in any desired direction, and, with just two coils, one obtains adequate control over the target location to scan the primary motor cortex (M1) without coil movement. To demonstrate practical electronic targeting, we built such a two-coil mTMS device and applied it to M1 *in vivo*.

Material and methods

Transducer design algorithm

For the design of mTMS transducers, we propose an algorithm that gives a close-to-minimum number of coils to obtain the desired degrees of freedom for electronic control of the characteristics of the E-field, such as the location of its maximum. The algorithm translates the problem into a matrix form and uses known matrix factorisation methods to minimise the number of coils needed to meet given specifications.

An N-channel mTMS transducer consists of a set of N coil windings, each with a different pattern of induced E-field. To find a suitable set of N coils, we first specify the spatial stimulation patterns the transducer should be able to produce. For simplicity, we define each stimulation pattern by the maximum induced E-field, $\boldsymbol{E}_{\text{target}}$ obtained at location $\boldsymbol{x}_{\text{target}}$, and its focality, that is, the extent of N_{ROI} regions outside of which the E-field magnitude is below certain thresholds [18]:

$$\boldsymbol{E}(\boldsymbol{x}_{\text{target}}) = \boldsymbol{E}_{\text{target}} ,$$

$$\forall \boldsymbol{x} \ : |\boldsymbol{E}(\boldsymbol{x})| \leq |\boldsymbol{E}_{\text{target}}| \text{ , and}$$

$$\forall \boldsymbol{x} \notin \text{ROI}_i \ : |\boldsymbol{E}(\boldsymbol{x})| \leq c_i |\boldsymbol{E}_{\text{target}}| .$$

ROI_i specifies the i:th region ($i = 1 \ldots N_{\text{ROI}}$) and $0 < c_i < 1$ describes how much the E-field amplitude is reduced outside it. For example, to design a transducer that is able to induce an equally focal E-field distribution in any orientation in any location within a continuous region of interest, we could form a nearly uniform grid of target locations and a set of equally spaced stimulation orientations for each target. When the discretised set of stimulation patterns has a sufficient sampling density, this set allows approximating a continuous set of target locations and orientations.

If we assume that the N coils forming the mTMS transducer are contained within one thin layer, each of them can be described in a common basis: as with our previous work, a coil is described by its stream function lying on a surface that follows the overall transducer shape and covers the whole transducer [19]. At this point, we define the overall shape of the transducer, e.g., planar or curved, and its dimensions. A stream function describes the amount of current around each point; any coil-current pattern can be approximately represented by an n-dimensional vector, $\boldsymbol{c}$, where n is the number of interior vertices in the triangular mesh used to discretise the surface. Next, we look for a set of coil-current patterns on the transducer surface that can induce all required stimulation patterns. The final N stream functions that correspond to the N coils of the transducer must span this set of coil-current patterns. We can obtain one possible set by computing the minimum-energy TMS coils, that is, solving the convex single-coil optimisation problem of Ref. [19], for all m specified stimulation patterns separately:

$$\arg\min_{\boldsymbol{c}_i \in C_i} \iiint |\boldsymbol{B}_{\boldsymbol{c}_i}(\boldsymbol{x})|^2 d\boldsymbol{x}^3 ,$$

where $\boldsymbol{c}_i$ is the minimum-energy coil from the set of all coils that satisfy the i:th pattern (C_i), $\boldsymbol{x}$ is a point in space, $\boldsymbol{B}_{\boldsymbol{c}_i}$ is the magnetic field due to coil $\boldsymbol{c}_i$, and the integration is carried over all space. From this, typically large set of coil-current patterns, we obtain a practical set by forming an n-by-m matrix $\mathbf{C}$ in which the coil-current patterns are columns,

$$\mathbf{C} = [\boldsymbol{c}_1 \boldsymbol{c}_2 \ldots \boldsymbol{c}_m] ,$$

computing its singular-value decomposition,

$$\mathbf{C} = \mathbf{U} \, \mathbf{\Sigma} \, \mathbf{V}^{\mathrm{T}} ,$$

and then taking the first N left singular vectors $\boldsymbol{u}_i$. Each of these singular vectors describes a coil-current pattern. When N is sufficiently large, linear combinations of $\boldsymbol{u}_i$ ($i = 1 \ldots N$) can approximate any of the original coil-current patterns $\boldsymbol{c}_i$ ($i = 1 \ldots m$).

Each singular vector $\boldsymbol{u}_i$ ($i = 1 \ldots N$) corresponds to a stream function that describes a particular transducer coil. As the $\boldsymbol{u}_i$ are mutually orthogonal, we can expect the corresponding coils to have near-zero mutual inductances. The coil windings can be extracted from the stream functions as in Refs. [18,19]: the individual turns of the windings follow the isolines of the stream functions, and the windings are obtained by connecting consecutive turns in a spiral-like fashion. However, as all coils are described in a common basis, their windings typically intersect; we can obtain feasible coil windings by adding a unique offset to each coil surface before extracting the windings. When offsetting a surface, it is useful to recompute the respective stream function to ensure that the E-field remains intact. This can be done by computing on the shifted surface the minimum-energy coil that induces the same E-field distribution as the original (unshifted) stream function using the single-coil optimisation method [19]. If there are a few thin coils, the re-optimisation makes typically little difference, and one can simply translate the stream functions (or the coil windings) by the required few millimetres. Note that the order of the coils affects the total efficiency of a transducer. As a rule of thumb, coils with the smallest characteristic size are most sensitive to the offset and should be placed closest to the head if all coils require similar maximum power levels—otherwise, coils with the lowest maximum power level can be placed farthest from the head. The number of turns in each coil can be selected independently. However, the maximum number of turns in one layer is limited by the wire thickness; if the desired level of inductance cannot be reached with this number of turns, inductance may be increased by adding turns of wire in series in another layer.

Thus, our algorithm to find a set of coil windings is as follows:

1. Form an evenly discretised set of stimulation patterns from the set of all desired stimulation patterns and build optimisation constraints for each pattern.
2. Select a suitable overall transducer shape. With a common basis, compute the stream function for the minimum-energy current pattern for each desired stimulation pattern.
3. Concatenate the stream functions that describe the minimum-energy coils into a matrix (the stream functions as its columns) and compute its singular value decomposition. Select the first N (here, $N = 2$) left singular vectors.
4. Test if the desired set of stimulation patterns can be sufficiently reproduced with the selected vectors. If not, either increase N or reduce the extent of the desired set of stimulation patterns.
5. Build N overlapping coil surfaces separated by the height of the coil windings. For each surface, design a minimum-energy coil producing the same E-field distribution as one of the coils described by the singular vectors.

We investigated the performance of the algorithm by designing transducers that can translate the stimulated spot within various regions. First, we determined a set of coils that can control both the orientation and location of the stimulated spot within a small region of the brain (similar to the region accessible with a lattice of 16 small round coils). We computed the induced E-field in the cortex in a spherical head model with 70-mm cortical radius and 85-mm outer radius using an analytical closed-form solution [20] and reciprocity [21], and used a large planar surface for the overall transducer shape. The computed stream functions matched the E-field distribution of a Magstim 70 mm Double Coil (The Magstim Co Ltd, www.magstim.com), which was modelled based on the model by Thielscher and Kammer [22]. The coil was translated and rotated to stimulate different spots within a rectangular region, the size of which was increased until the required number of coils increased. The points in the region were sampled from a geodesic polyhedron whose edge lengths ranged from 2.4 to 2.9 mm. In each point, the different orientations were sampled with 30° steps, and the focality constraints for each E-field distribution were defined at 70, 90, 95, 99, and 100% of the peak E-field. Second, we studied how the number of coils increases when the surface area of the accessible region is doubled. Third, we investigated a limiting case by designing a transducer for the stimulation of the whole superficial cortex, with a coil surface that covers the scalp in a spherically symmetric head model (i.e., a hemispherical surface). Note that, although in this study we applied the spherically symmetric head geometry, the design formalism applies also to realistic head geometry [19]. In this study, we calculated E-fields in a spherical head model as opposed to a realistic head model, as these two approaches produce nearly identical coils for the stimulation of motor areas (see Refs. [18,19]). In addition, coil optimisation in the spherical head model requires only about 1% of the computation time compared to that with realistic head models. The much faster computation is mainly due to much simpler 2-dimensional focality constraints (in each discretisation point, 16 and 162 linear constrains are required to approximate the constraint for the E-field magnitude in 2 and 3 dimensions, respectively, see Ref. [19]).

Two-coil transducer design and implementation

We designed and built a multi-locus transducer that can translate the stimulated spot along a 30-mm-long line segment perpendicular to the direction of the peak E-field. When designing this mTMS transducer, we computed the induced E-field in the geometry described in the previous section, used a large planar surface for the overall transducer shape, and computed 31 stream functions to match the E-field distribution of a Magstim 70 mm Double Coil that was translated to stimulate different spots from −15 to 15 mm in 1-mm steps. The focality constraints for each E-field distribution were defined at 70, 90, 95, 99, and 100% of the peak E-field. The first two singular vectors ($\boldsymbol{u}_1$ and $\boldsymbol{u}_2$) explained most (88%) of the variance in this 31-dimensional system. We extracted coil windings from these two vectors, with the number of turns selected so that the inductance of both coils with two strands of wire per turn in series was between 16 and 18 μH. The oval coil, described by $\boldsymbol{u}_2$, was translated outwards by 4 mm to avoid intersecting windings.

We manufactured a coil former from a 10-mm-thick 300-by-200-mm-wide sheet of polyvinyl chloride following the description of Ref. [19]. The wiring of the figure-of-eight coil was placed at the bottom of machined 9-mm-deep grooves; the oval coil was wound on top of it in 5-mm-deep grooves. Each coil had two strands of Litz wire (70 circular 0.2-mm-thick strands, Rudolf Pack GmbH & Co. KG, www.pack-feindraehte.de) in series. Finally, the wires were glued with epoxy and connected to coil cables. The transducer was finished by assembling a 5-mm-thick polyvinyl-chloride lid with an attached commercial navigation unit (Nexstim eXimia Navigated Brain Stimulation System, www.nexstim.com).

mTMS device

We also designed and built a two-channel mTMS device. The device comprises control and power electronics for both channels, which are essentially copies of our custom-made TMS design [19]. This mTMS device allows similar pulse waveforms in both coils: it features controllable-pulse-waveform electronics similar to the design of Peterchev et al. [23] with high capacitance and near-rectangular pulse waveforms, the pulse duration being independent of the coil inductance. The device comprises two insulated-gate bipolar transistor (ABB 5SNA 1500E330305, www.abb.com) H-bridge circuits with one 1020-μF capacitor (Electronicon E50.R34-105NT0, www.electronicon.com) for each. In addition to the H bridges, the system has a common high-voltage power supply (Lumina Power CCPF-2000, www.luminapower.com), which is shared between the two channels via a custom-made solid-state relay board, and a common control with a real-time field-programmable gate array hardware (National Instruments PXI-7841R, www.ni.com). Both capacitors have their own resistive discharge systems. The mTMS device is interfaced with a custom-made LabVIEW program (National Instruments).

Validation

We used our TMS-coil characteriser [24], which provides E-field values in a spherical head model with 70-mm cortical radius and 85-mm outer radius, to measure E-field distributions of the two-coil transducer when driven by our mTMS device. These measurements were used to determine the mutual inductance between the two coils and to fine-tune the coil voltages to obtain the same E-field intensity for all translations. In addition, we measured the E-field distributions of each coil individually (with the other coil disconnected from the device) to estimate the accuracy of the manufacturing process of the coils.

In vivo demonstration

Two healthy males (33 and 28 years old, one left-handed) with no contraindication for TMS participated in the study after giving their written informed consents. The study was approved by the Coordinating Ethics Committee of the Hospital District of Helsinki

and Uusimaa and was carried out in accordance with the Declaration of Helsinki.

During the study, the subject sat in a chair and was instructed to keep his right hand relaxed. We recorded electromyography (EMG) from the right *abductor pollicis brevis* (APB) muscle with surface electrodes connected to an EMG device (Nexstim eXimia). The device had a 500-Hz low-pass filter and 3000-Hz sampling frequency.

First, using only the figure-of-eight coil and physically moving the two-coil transducer, we determined the right APB hotspot by finding the location in the left primary motor cortex that produced the largest motor-evoked potentials (MEP) at a given stimulation intensity. Then, we measured the resting motor threshold (RMT) as the lowest stimulation intensity that produced MEPs greater than or equal to 50 μV in peak-to-peak amplitude in at least 10 out of 20 consecutive trials [25]. Finally, we mapped the APB motor representation area in two ways: (1) Conventional mapping was carried out by using only the figure-of-eight coil and physically moving the two-coil transducer to stimulate different targets around the APB hotspot (a total of 150 pulses). (2) Electronically controlled mapping was conducted by holding the coil in place and electronically translating the stimulated spot in randomised order from −15 to 15 mm relative to the APB hotspot in 1-mm steps (a total of 124 pulses). In both mappings, the stimulation intensity was 110% RMT. For subject 1, the conventional mapping was performed first, whereas for subject 2, the electronic mapping was performed first. All TMS pulses delivered with our custom-made mTMS device were monophasic with a 60-μs rise time and a 30-μs "hold period" of near-constant current [26]; the interstimulus interval was randomised between 4 and 6 s.

The transducer position relative to the head was measured with a neuronavigation system (Nexstim eXimia Navigated Brain Stimulation System). This system was used both to estimate the stimulated spots in the conventional mapping and to maintain a constant coil position and orientation during the RMT measurement and during the electronic mapping. The apparent change in the location of the stimulated spot was defined as the Cartesian distance between the predicted cortical locations of the E-field maximum in the cortex. In the navigation software, we selected the most similar coil to our figure-of-eight coil, the Magstim 70 mm Double Coil.

We rejected trials containing muscle preactivation, artefacts, or noise exceeding ±10 μV in amplitude in the 100-ms time window preceding TMS (a total of 2 out of 548 trials were rejected); in addition, we rejected the trials in which the coil location was not recorded (a total of 4 out of the remaining 546 trials were rejected). In the accepted trials, we determined the MEP peak-to-peak amplitudes. To assess the similarity of the conventional and electronic mapping, for both subjects, we determined the width of a region that produced MEPs greater than or equal to 50 μV in peak-to-peak amplitude. First, we took the moving median of ten consecutive responses. Then, to account for possibly discontinuous regions, we computed the distances between the farthest-from-origin points with median greater than or equal to 50 μV and the closest-to-origin points with median less than 50 μV. Finally, we defined the width of the region as the mean of these two distances. We compared the widths obtained by conventional and electronic mapping with a permutation test (1,000 repetitions, uncorrected two-tailed comparison). The level of statistical significance was chosen to be $P < 0.05$.

Results

Transducer design algorithm

For controlling both the stimulation direction and the location of the stimulated spot within a relatively small region of the cortex, the algorithm yields a set of five overlapping coils: two figure-of-eight coils at a 90° angle, a circular coil, and two four-leaf-clover coils at a 45° angle (Fig. 1). The possible E-field maxima produced by this set of coils cover a cortical region of approximately 30-by-30 mm^2.

All five coils of the transducer shown in Fig. 1 resemble coils that have been used for TMS [1,7] or magnetic nerve stimulation [27] and are also reasonably efficient unlike small circular coils. From this five-coil set, three useful two-coil subsets can be identified. (1) Two figure-of-eight coils can control the orientation of the stimulation (Fig. 1a and b). (2) A figure-of-eight coil and a matched four-leaf-clover coil can control the location of the stimulated spot in the direction parallel to the stimulation direction (e.g., Fig. 1a and e). (3) A figure-of-eight coil and a matched, somewhat circular coil can control the location of the stimulated spot in the direction perpendicular to the stimulation direction (e.g., the coil in Fig. 1a and a coil formed by merging the coils in Fig. 1c and d; see Fig. 2). As the primary motor cortex is often stimulated in the direction

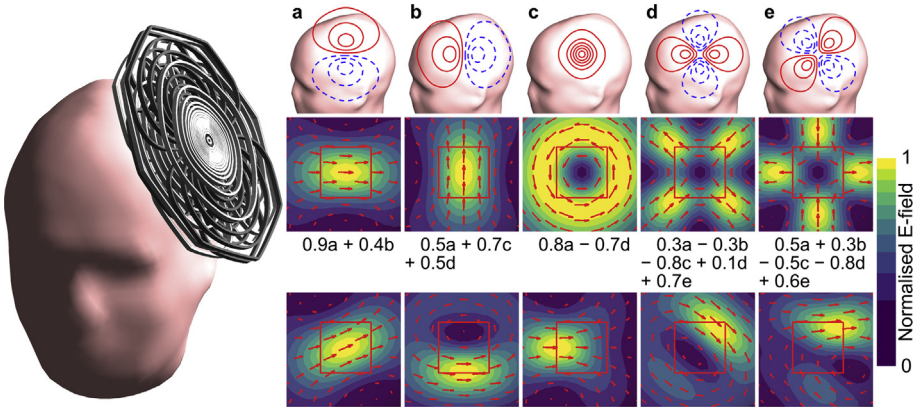

Fig. 1. Five-coil mTMS transducer. With five coils, the location of the stimulated spot can be moved in both tangential directions and the stimulation direction can be freely selected. **(a–e)** The coil windings of each coil are shown with a reduced number of turns for increased clarity. The solid red and the dashed blue windings carry current in clockwise and counter-clockwise directions for positive coil voltages, respectively. Each coil induces a distinct E-field distribution in the cortex (middle row). Their superpositions produce the desired stimuli, some examples of which are shown in the bottom row. The side lengths of the red squares are 30 mm. The E-field distributions were computed in the spherical head model described in section "Transducer design algorithm" and a realistic head model is used to illustrate better the size of the resulting coils. The visualisation on the left shows all five coils assembled into a single transducer; in the visualisation, the coils are in order e–d–b–a–c to maximise the total system efficiency. (For interpretation of the references to colour in this figure legend, the reader is referred to the Web version of this article.)

perpendicular to the central sulcus, this last pair alone would already provide most of the desired control over the stimulated spot in the primary motor cortex.

In addition to smaller regions of interest, the algorithm is suitable for designing optimised coil sets for larger regions of interest. For example, the size of the covered region can be doubled by increasing the number of coils from five to eight. When one applies this algorithm to design a transducer for a wide region of interest, e.g., the whole superficial cortex, with a coil surface that covers the scalp, the algorithm gives a set of increasingly complicated TMS coils, each of which would cover the whole transducer surface. With typical TMS focality constraints, about 50–70 such coils would suffice for adequate control. In this case, an orthogonal varimax rotation [28] of the coil-current patterns may be used to minimise their overlap and yield an array of small (near-) circular coils more suitable for practical implementation. Neighbours of such algorithmically designed small coils overlap by about 10% to remain orthogonal and to provide smooth control over the stimulated spot. In addition, the coils at the edge of the array have about twice the surface area of the other coils.

Two-coil transducer

The two-coil transducer that can translate the stimulated spot along a 30-mm-long line segment perpendicular to the stimulation direction resembles a figure-of-eight coil overlaid by an oval coil (Fig. 2). Our figure-of-eight coil alone produces an E-field distribution similar to that of conventional figure-of-eight coils (Fig. 3b, solid purple line), whereas the oval coil produces a bimodal field distribution along its left–right axis, with opposite E-field directions (Fig. 3b, dashed green line). A superposition of these two E-fields can translate the peak induced E-field along the left–right axis of the transducer (e.g., as in Fig. 3b dotted black line). If the coil voltages in both coils are selected appropriately (Fig. 3a), we can maintain constant peak intensity while moving the stimulated spot steplessly (Fig. 3c).

The voltages shown in Fig. 3a were fine-tuned to compensate for the non-zero mutual inductance between the two coils, which we estimated to be around 0.02 times the coil inductance. The manufacturing process produced coils that were highly similar with their corresponding simulated properties: both measured field distributions in the direction perpendicular to the peak induced E-field of the figure-of-eight coil (Fig. 3b) are almost indistinguishable from the corresponding simulated spatial distributions of the coil windings (correlation 0.998 for the figure-of-eight coil and 0.999 for the oval coil).

In vivo demonstration

The conventional and the electronically controlled maps of the APB motor representation area had similar extent for both subjects, as seen in Fig. 4. For subject 1, the widths of the regions producing MEPs greater than or equal to 50 μV in peak-to-peak amplitude at 110% RMT in the conventional and electronic mappings were 13.7 and 16.8 mm, respectively. The difference between these two values was not statistically significant (uncorrected two-tailed $P = 0.074$). For subject 2, the respective values were 15.7 and 15.3 mm (uncorrected two-tailed $P = 0.83$). For subject 2, the maps are also visually essentially indistinguishable; for subject 1, the electronic map appears slightly wider than the conventional map. Ideally, the conventional and electronic mapping results should be similar to each other.

Discussion

We have proposed and demonstrated a practical approach to mTMS: overlapping coils forming a single transducer enable stepless electronic selection of the stimulated spot. This approach differs considerably from the previously suggested approach of having an array of adjacent coils [8,16], which would require considerably more channels in particular for the minimum viable array size. In addition, to allow stepless control over the stimulated spot, those adjacent coils would have to be relatively small and

Fig. 2. Two-coil mTMS transducer. Our transducer consists of a minimum-energy figure-of-eight coil and an overlapping oval coil. The figure-of-eight coil alone produces a focal stimulus underneath the centre of the transducer. The oval coil alone produces a relatively broad stimulus on both sides of that location, with the E-field reversing its direction underneath the centre of the transducer. As a superposition of the fields of the two coils, we obtain a focal stimulus to the desired target near the centre. After the photograph was taken, the wires were glued in place with epoxy.

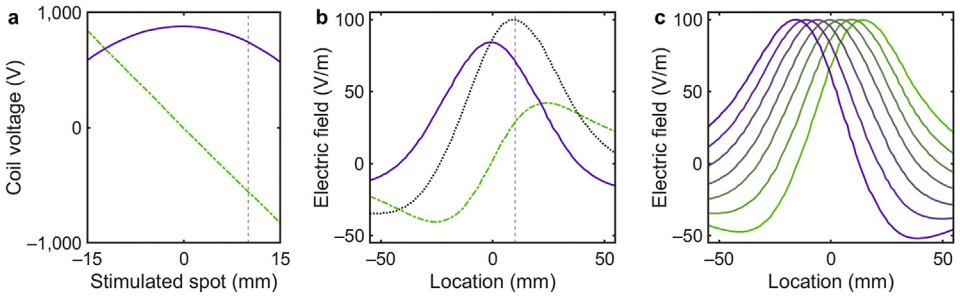

Fig. 3. Coil voltage and induced electric field. The stimulated spot can be adjusted by changing the voltages that drive the currents to the coils of our mTMS transducer. **(a)** The relationship between the location of the stimulated spot relative to the transducer centre and the coil voltage in the figure-of-eight coil is near-parabolic (solid purple curve); for the oval coil, this relationship is near-linear (dashed green curve). **(b)** A linear superposition of the E-field distributions of the figure-of-eight coil (solid purple line) and oval coil (dashed green line) produces an E-field distribution whose peak is translated (dotted black line). Here, the location is measured along a curved line perpendicular to the peak induced E-field in a spherical phantom. In **(a)** and **(b)**, the vertical dashed lines indicate the location of the stimulated spot of panel **(b)**. **(c)** The measured E-field distribution along a curved line perpendicular to the peak induced E-field in a spherical phantom when the stimulated spot is located at −15, −10, −5, 0, 5, 10, and 15 mm. When connected to the mTMS device, the two coils have a non-zero mutual inductance (coupling coefficient of the order of 0.02), which has been compensated for in the coil voltages **(a)** to produce constant stimulation intensity at all target positions **(c)**. (For interpretation of the references to colour in this figure legend, the reader is referred to the Web version of this article.)

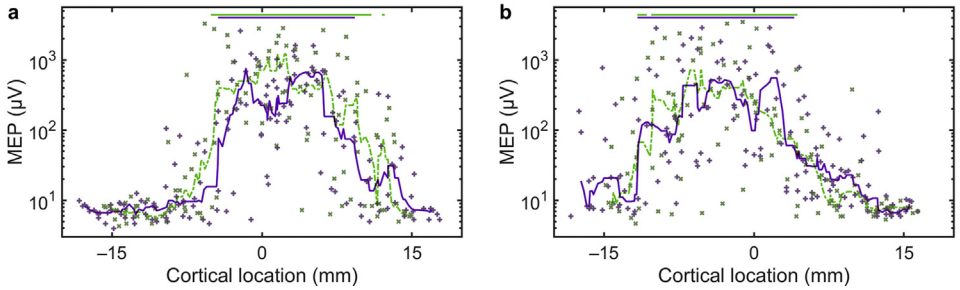

Fig. 4. Motor mapping. Panels **(a)** and **(b)** depict the MEP peak-to-peak amplitudes of subjects 1 and 2 as a function of the cortical location of the peak induced E-field, respectively. The solid purple lines and the dashed green lines visualise the conventional and electronic motor representation maps of the APB muscle (at 110% RMT), respectively. Each line depicts the median of ten consecutive individual responses, covering on average 2 mm of the cortex. The individual responses of the conventional and electronic mappings are represented with purple plusses and green crosses, respectively. A motor representation area (indicated by the horizontal purple and green lines near the top of the panels) is defined as the area in which the respective median curve is above 50 μV. The widths of the motor representation areas of the conventional and electronic maps do not differ in a statistically significant sense ($P = 0.074$ and $P = 0.83$ for subject 1 and 2, respectively). (For interpretation of the references to colour in this figure legend, the reader is referred to the Web version of this article.)

therefore inefficient—each of them alone would require similar levels of power as a single conventional TMS coil. The proposed approach solves both limitations; thus, with just two overlapping coils, we could build the simplest instance of an electronically controlled mTMS device that allows shifting the stimulated spot while keeping the E-field profile essentially unchanged.

Our *in vivo* demonstration of the electronic stimulation targeting showed that physical transducer movement can be substituted with electronic targeting. For subject 2, the two mapping approaches produced practically identical results. The slight differences in the mapping results of subject 1 may be due to several reasons, e.g., a higher excitability of the M1 during the electronic mapping. Indeed, the electronic mapping produced larger responses than the conventional mapping at the cortical location 0 (see Fig. 4a) although this corresponds to identical stimulation with the figure-of-eight coil only in both methods.

The electronic control can be made near instantaneous compared to the time scales at which the brain functions; the described mTMS device can stimulate separate cortical targets with interstimulus intervals down to around 0.3 ms (the lower limit of the interstimulus interval is given by the TMS-pulse duration). Thus, electronically controlled mTMS allows, for example, studying short-distance interactions between inhibitory and facilitatory circuits [14] in detail. When combined with physiological or behavioural recordings, mTMS would allow implementing also closed-loop paradigms [29–31], in which the stimulation targets and timings of subsequent pulses would be derived, e.g., from real-time-analysed electroencephalography data.

In addition to its impact on neuroscience, the ability to select different stimulation targets without any physical movement of the transducer may revolutionise also clinical TMS. mTMS will allow, e.g., electronic stabilisation to compensate for minor patient movements during a treatment session. This would reduce the stress of manual effort required to maintain the correct coil position. In addition, mTMS devices with electronic control over the stimulated spot would allow automating clinical procedures in which cortical areas are mapped, e.g., before brain surgery [32,33]. With the development of new mTMS paradigms, we anticipate that mTMS will lead to new clinical applications.

Conclusions

We developed an algorithm to design practical mTMS transducers capable of electronic stimulation targeting and demonstrated such a transducer *in vivo*.

Acknowledgements

This work was supported by the Finnish Cultural Foundation and the Academy of Finland (Decision Nos. 255347, 265680, and 294625). The coil former parts were manufactured by Enna Rane (Aalto University Design Factory). The coil cables and their

connectors were donated by Nexstim Plc. We acknowledge the computational resources provided by the Aalto Science-IT project.

Conflicts of interest

The authors are inventors on patent applications on mTMS technology. J.O.N. has received unrelated consulting fees from Nexstim Plc., and R.J.I. is an advisor and a minority shareholder of the company.

References

[1] Barker AT, Jalinous R, Freeston IL. Non-invasive magnetic stimulation of human motor cortex. Lancet 1985;325:1106–7.

[2] Massimini M, Ferrarelli F, Huber R, Esser SK, Singh H, Tononi G. Breakdown of cortical effective connectivity during sleep. Science 2005;309:2228–32.

[3] Reis J, Swayne OB, Vandermeeren Y, Camus M, Dimyan MA, Harris-Love M, et al. Contribution of transcranial magnetic stimulation to the understanding of cortical mechanisms involved in motor control. J Physiol 2008;586:325–51.

[4] Rose NS, LaRocque JJ, Riggall AC, Gosseries O, Starrett MJ, Meyering EE, et al. Reactivation of latent working memories with transcranial magnetic stimulation. Science 2016;354:1136–9.

[5] Berlim MT, van den Eynde F, Tovar-Perdomo S, Daskalakis ZJ. Response, remission and drop-out rates following high-frequency repetitive transcranial magnetic stimulation (rTMS) for treating major depression: a systematic review and meta-analysis of randomized, double-blind and sham-controlled trials. Psychol Med 2014;44:225–39.

[6] Lefaucheur JP, Picht T. The value of preoperative functional cortical mapping using navigated TMS. Clin Neurophysiol 2016;46:125–33.

[7] Ueno S, Tashiro T, Harada K. Localized stimulation of neural tissues in the brain by means of a paired configuration of time-varying magnetic fields. J Appl Phys 1988;64:5862–4.

[8] Ruohonen J, Ilmoniemi RJ. Multichannel magnetic stimulation: improved stimulus targeting. Adv Occup Med Rehabil 1996;2:55–64.

[9] Ettinger GJ, Leventon ME, Grimson WEL, Kikinis R, Gugino L, Cote W, et al. Experimentation with a transcranial magnetic stimulation system for functional brain mapping. Med Image Anal 1998;2:133–42.

[10] Karhu J, Hannula H, Laine J, Ruohonen J. Navigated transcranial magnetic stimulation: principles and protocol for mapping the motor cortex. In: Rotenberg A, Horvath JC, Pascual-Leone A, editors. Transcranial magnetic stimulation. New York: Springer; 2014. p. 337–59.

[11] Kantelhardt SR, Fadini T, Finke M, Kallenberg K, Siemerkus J, Bockermann V, et al. Robot-assisted image-guided transcranial magnetic stimulation for somatotopic mapping of the motor cortex: a clinical pilot study. Acta Neurochir 2010;152:333–43.

[12] Kujirai T, Caramia MD, Rothwell JC, Day BL, Thompson PD, Ferbert A, et al. Corticocortical inhibition in human motor cortex. J Physiol 1993;471:501–19.

[13] Arai N, Müller-Dahlhaus F, Murakami T, Bliem B, Lu MK, Ugawa Y, et al. State-dependent and timing-dependent bidirectional associative plasticity in the human SMA-M1 network. J Neurosci 2011;31:15376–83.

[14] Ziemann U, Rothwell JC, Ridding MC. Interaction between intracortical inhibition and facilitation in human motor cortex. J Physiol 1996;496:873–81.

[15] Bäumer T, Schippling S, Kroeger J, Zittel S, Koch G, Thomalla G, et al. Inhibitory and facilitatory connectivity from ventral premotor to primary motor cortex in healthy humans at rest – a bifocal TMS study. Clin Neurophysiol 2009;120:1724–31.

[16] Ilmoniemi RJ, Grandori, F. Device for applying a programmable excitation electric field to a target, Patent FI 100458 B, filed October 13, 1993, issued December 15, 1997.

[17] Roth BJ, Maccabee PJ, Eberle LP, Amassian VE, Hallett M, Cadwell J, et al. *In vitro* evaluation of a 4-leaf coil design for magnetic stimulation of peripheral nerve. Electroencephalogr Clin Neurophysiol 1994;93:68–74.

[18] Koponen LM, Nieminen JO, Ilmoniemi RJ. Minimum-energy coils for transcranial magnetic stimulation: application to focal stimulation. Brain Stimul 2015;8:124–34.

[19] Koponen LM, Nieminen JO, Mutanen TP, Stenroos M, Ilmoniemi RJ. Coil optimisation for transcranial magnetic stimulation in realistic head geometry. Brain Stimul 2017;10:795–805.

[20] Sarvas J. Basic mathematical and electromagnetic concepts of the biomagnetic inverse problem. Phys Med Biol 1987;32:11–22.

[21] Heller L, van Hulsteyn DB. Brain stimulation using electromagnetic sources: theoretical aspects. Biophys J 1992;63:129–38.

[22] Thielscher A, Kammer T. Linking physics with physiology in TMS: a sphere field model to determine the cortical stimulation site in TMS. Neuroimage 2002;17:1117–30.

[23] Peterchev AV, D'Ostilio K, Rothwell JC, Murphy DL. Controllable pulse parameter transcranial magnetic stimulator with enhanced circuit topology and pulse shaping. J Neural Eng 2014;11:056023.

[24] Nieminen JO, Koponen LM, Ilmoniemi RJ. Experimental characterization of the electric field distribution induced by TMS devices. Brain Stimul 2015;8:582–9.

[25] Rothwell JC, Hallett M, Berardelli A, Eisen A, Rossini P, Paulus W. Magnetic stimulation: motor evoked potentials. Electroencephalogr Clin Neurophysiol Suppl 1999;52:97–103.

[26] Koponen LM, Nieminen JO, Mutanen TP, Ilmoniemi RJ. Non-invasive extraction of microsecond-scale dynamics from human motor cortex. Hum Brain Mapp. https://doi.org/10.1002/hbm.24010.

[27] Roth Y, Levkovitz Y, Pell GS, Ankry M, Zangen A. Safety and characterization of a novel multi-channel TMS stimulator. Brain Stimul 2014;7:194–205.

[28] Kaiser HF. The varimax criterion for analytic rotation in factor analysis. Psychometrika 1958;23:187–200.

[29] Bergmann TO, Karabanov A, Hartwigsen G, Thielscher A, Siebner HR. Combining non-invasive transcranial brain stimulation with neuroimaging and electrophysiology: current approaches and future perspectives. Neuroimage 2016;140:4–19.

[30] Zrenner C, Belardinelli P, Müller-Dahlhaus F, Ziemann U. Closed-loop neuroscience and non-invasive brain stimulation: a tale of two loops. Front Cell Neurosci 2016;10:92.

[31] Zrenner C, Desideri D, Belardinelli P, Ziemann U. Real-time EEG-defined excitability states determine efficacy of TMS-induced plasticity in human motor cortex. Brain Stimul 2018;11:374–89.

[32] Picht T, Schmidt S, Brandt S, Frey D, Hannula H, Neuvonen T, et al. Preoperative functional mapping for rolandic brain tumor surgery: comparison of navigated transcranial magnetic stimulation to direct cortical stimulation. Neurosurgery 2011;69:581–9.

[33] Picht T, Krieg SM, Sollmann N, Rösler J, Niraula B, Neuvonen T, et al. A comparison of language mapping by preoperative navigated transcranial magnetic stimulation and direct cortical stimulation during awake surgery. Neurosurgery 2013;72:808–19.